

See discussions, stats, and author profiles for this publication at: <https://www.researchgate.net/publication/263956456>

Bi₂O₂CO₃/BiOI Photocatalysts with Heterojunctions Highly Efficient for Visible-Light Treatment of Dye-Containing Wastewater

ARTICLE in INDUSTRIAL & ENGINEERING CHEMISTRY RESEARCH · MAY 2012

Impact Factor: 2.59 · DOI: 10.1021/ie300567y

CITATIONS

84

READS

187

7 AUTHORS, INCLUDING:



Lang Chen

Hunan University

31 PUBLICATIONS 450 CITATIONS

[SEE PROFILE](#)



Tao Hong

University of Tennessee

3 PUBLICATIONS 84 CITATIONS

[SEE PROFILE](#)

Bi₂O₂CO₃/BiOI Photocatalysts with Heterojunctions Highly Efficient for Visible-Light Treatment of Dye-Containing Wastewater

Lang Chen,[†] Shuang-Feng Yin,^{*,†} Sheng-Lian Luo,[†] Rui Huang,[†] Qiang Zhang,[†] Tao Hong,[†] and Peter C.T. Au^{‡,§}

[†]College of Chemistry and Chemical Engineering, Hunan University, Changsha 410082, Hunan, China

[‡]Department of Chemistry, Hong Kong Baptist University, Kowloon Tong, Hong Kong

Supporting Information

ABSTRACT: Bi₂O₂CO₃/BiOI composites were fabricated at room temperature for the first time by a facile method. X-ray diffraction (XRD), X-ray photoelectron spectroscopy (XPS), scanning electron microscopy (SEM), transmission electron microscopy (TEM), UV-vis diffuse reflectance spectra (UV-vis DRS), and nitrogen adsorption-desorption techniques were employed to characterize the physiochemical properties of the composites. The photocatalytic activities of Bi₂O₂CO₃, BiOI, and Bi₂O₂CO₃/BiOI were evaluated through the photocleaning of wastewater which contained rhodamine-B, methylene blue, crystal violet, or a mixture of them under visible-light irradiation ($\lambda \geq 420$ nm). The photocatalytic activity of Bi₂O₂CO₃/BiOI is much higher than that of its components. Moreover, the composite shows good photostability and recyclability. The excellent catalytic efficiency of the Bi₂O₂CO₃/BiOI composite is deduced closely related to Bi₂O₂CO₃/BiOI heterojunctions whose presence is generally regarded to be a favorable factor for the separation of photogenerated electrons and holes. Moreover, ·OH was found to be the main active species for the photocatalytic interactions. The catalyst shows potential application in the treatment of dye-containing wastewater.

INTRODUCTION

Photocatalysis has been a hot research area for the utilization of solar energy.^{1,2} In recent years, much attention has been paid to H₂ generation from water and degradation of organic contaminants.^{3–8} Besides the semiconductor photocatalysts, composite photocatalysts have been studied as well.^{9,10} Due to the formation of heterojunctions that can significantly reduce the recombination and speed up the separation rate of photogenerated charge carriers, the composites are photocatalytically more active than the individual components. A lot of composites have been synthesized, such as Bi@Bi₂O₃ microspheres,¹¹ three-dimensional Bi₂WO₆/TiO₂,¹² BiOI/TiO₂,^{13,14} AgI/BiOI,¹⁵ BiOCl/Bi₂O₃,¹⁶ NaBiO₃/BiOCl,¹⁷ BiOCl/BiOI,¹⁸ TiO₂/SnO₂,¹⁹ ZnO/In₂O₃,²⁰ and core/shell BiVO₄@Bi₂O₃.²¹ Nonetheless, the structures of heterojunctions are complex, and the fabrication of composite photocatalysts with band gap specificity remains as a big challenge.

On the basis of the results of extensive investigations, it is generally agreed that the coupling of two semiconductor photocatalysts would result in better photocatalytic activities.^{14,20,21} Among the reported photocatalysts, the bismuth-containing ones such as Bi₂O₃,^{22–25} Bi₂WO₆,^{26–28} BiVO₄,^{29,30} and BiOX (X = Cl, Br, I)^{31–34} aroused much interest because they respond to visible light. These Bi-based materials all belong to the layered or Aurivillius-related oxide family with characteristic structures of alternative stacking of (Bi₂O₂)²⁺ layers and slabs of other inorganic atoms or groups. As a member of this family, Bi₂O₂CO₃ has long been used for medical and healthcare purpose.³⁵ Cheng et al.³⁶ reported for the first time the use of Bi₂O₂CO₃ as a photocatalyst in degradation of methyl orange (MO) in aqueous solution under UV light irradiation. Since then, Bi₂O₂CO₃ was used as

photocatalysts in rhodamine-B (Rh-B) degradation and showed high activity under the irradiation of solar light generated by a 300W and 1000W Xe lamp without a cut filter.^{37,38} The band gap of Bi₂O₂CO₃ is 3.55 eV,³⁸ with such a wide band gap, the semiconductor only functions well under UV light or artificial sun light. As another member of the Aurivillius-related oxide family, bismuth oxyhalides (BiOX, X = Cl, Br, I) have narrow band gaps and are potential visible-light photocatalysts.^{31–34} For example, BiOI has a band gap of 1.7–1.83 eV and can absorb most of the visible light ($\lambda < 700$ nm). However, by itself, BiOI is always poor in photocatalytic activity.^{33,34} In view of the fact that Bi₂O₂CO₃ and BiOI are similar in structure, it is envisaged that a Bi₂O₂CO₃/BiOI composite can have the merits of Bi₂O₂CO₃ and BiOI, consequently showing high photocatalytic activity under visible light.

In this paper, Bi₂O₂CO₃/BiOI composites were fabricated at room temperature (RT) by a facile method with the assistance of hexadecyltrimethylammonium bromide (CTAB). The as-synthesized composites were examined in the photocatalytic degradation of Rh-B, MB, and/or crystal violet under visible-light irradiation. The correlation between the catalytic performance and structure of the photocatalyst was also investigated.

EXPERIMENTAL SECTION

Synthesis of Catalyst. All the reagents are of analytic grade and used without further purification. In a typical process, 4.85

Received: March 2, 2012

Revised: April 8, 2012

Accepted: April 25, 2012

Published: April 25, 2012



g $\text{Bi}(\text{NO}_3)_3 \cdot 5\text{H}_2\text{O}$ (10 mmol) was dissolved in 10 mL of HNO_3 (1 mol/L) to get a transparent solution (named as solution A). Also, 0.5 g of CTAB and a proper amount of Na_2CO_3 and NH_4I were diluted in 140 mL of distilled water (molar ratio of $\text{Bi}^{3+}/\text{CO}_3^{2-}/\text{I}^- = 1/8/0, 1/7/1, 1/6/2, 1/4/4$, and $1/0/2$) to obtain a transparent solution (named as solution B). Solution A was added dropwise into B with constant stirring, and there was the immediate precipitation of product. The mixture was kept stirring for 10 min before the resulting precipitate was collected and washed several times with distilled water and absolute alcohol. The as-synthesized $\text{Bi}_2\text{O}_2\text{CO}_3/\text{BiOI}$ composites were dried at 80 °C for 4 h.

Characterization. A powder X-ray diffraction (XRD) experiment was conducted on a Bruker Automatic Diffractometer (Bruker D8 Advance) with monochromatized Cu $\text{K}\alpha$ radiation ($\lambda = 0.15406$ nm) at a setting of 40 kV and 80 mA. The scanning rate was 0.02° (2θ)/s, and the scanning range was 5 – 75° . The binding energy of Bi, O, C, and I were measured at RT using X-ray photoelectron spectroscopy (XPS, SSX-100, Mg $\text{K}\alpha$), and the relevant peak position was calibrated against the C1s signal (284.6 eV) of contaminant carbon. The morphology of as-prepared samples was examined using a field emission scanning electron microscope (FE-SEM) (Hitachi S-4800) equipped with an energy-dispersive spectroscopic (EDS) device. Transmission electron microscopy (TEM) and high-resolution transmission electron microscopy (HRTEM) images were taken over a JEM-3010F transmission electron microscope. The BET surface area was measured using a Micromeritics 2010C instrument. The UV-vis diffuse reflectance spectra (UV-vis DRS) of samples were obtained over a UV-vis spectrophotometer (Cary 300) using BaSO_4 as reference.

Photocatalytic Activity Evaluation. Rh-B, MB, and crystal violet were used as probe dyes to evaluate the activity of the as-prepared $\text{Bi}_2\text{O}_2\text{CO}_3/\text{BiOI}$ catalysts. Typically, 0.05 g of catalyst and 100 mL of aqueous solution containing of Rh-B, MB, or crystal violet (2×10^{-5} mol/L) were added into a homemade Pyrex glass vessel with temperature being maintained at RT during reaction by means of an external water flow. The mixture was kept stirring in the dark using a magnetic bar for 30 min (to establish adsorption–desorption equilibrium between catalysts and dye molecules). Afterward, the contents were exposed to visible light ($\lambda \geq 420$ nm) originated from a 350 W Xe lamp with a 420 nm cutoff filter. The distance between the light and the liquid surface was set at 25 cm. The content was sampled (about 4 mL) at selected intervals. The catalyst in the mixture was removed by centrifugation (4000 r/min for 3 min), and the residual dyes in the solution were determined over a Cary-300 UV-vis spectrophotometer.

RESULTS AND DISCUSSION

XRD Patterns. Figure 1 shows the XRD patterns of $\text{Bi}_2\text{O}_2\text{CO}_3$, BiOI, and the $\text{Bi}_2\text{O}_2\text{CO}_3/\text{BiOI}$ composites with different $\text{Bi}^{3+}/\text{CO}_3^{2-}/\text{I}^-$ molar ratios. The diffraction peaks of Figure 1a,f can be indexed to tetragonal phase $\text{Bi}_2\text{O}_2\text{CO}_3$ (JCPDS card No. 41-1488) and tetragonal phase BiOI (JCPDS card No. 73-2062), respectively, and there was no detection of impurities. The narrow and sharp peaks indicate high crystallinity of $\text{Bi}_2\text{O}_2\text{CO}_3$ and BiOI. It is clear that, as the amount of BiOI increases in the composites (Figure 1b,d,e), all the diffraction peaks of $\text{Bi}_2\text{O}_2\text{CO}_3$ become wider; also there is no appearance of peaks that can be indexed to BiOI or

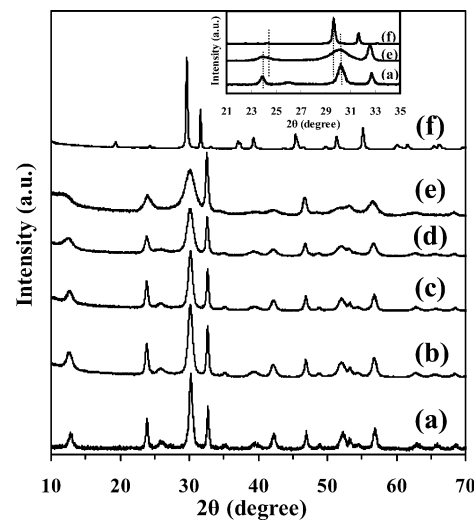


Figure 1. XRD patterns of as-prepared samples: (a) $\text{Bi}_2\text{O}_2\text{CO}_3$, (b) $\text{Bi}_2\text{O}_2\text{CO}_3/\text{BiOI}$ ($\text{Bi}^{3+}/\text{CO}_3^{2-}/\text{I}^- = 1/7/1$), (c) $\text{Bi}_2\text{O}_2\text{CO}_3/\text{BiOI}$ ($\text{Bi}^{3+}/\text{CO}_3^{2-}/\text{I}^- = 1/7/1$) after the 10th run, (d) $\text{Bi}_2\text{O}_2\text{CO}_3/\text{BiOI}$ ($\text{Bi}^{3+}/\text{CO}_3^{2-}/\text{I}^- = 1/6/2$), (e) $\text{Bi}_2\text{O}_2\text{CO}_3/\text{BiOI}$ ($\text{Bi}^{3+}/\text{CO}_3^{2-}/\text{I}^- = 1/4/4$), and (f) BiOI.

impurities. However, from the inset of Figure 1, one can see that with the broadening of $\text{Bi}_2\text{O}_2\text{CO}_3$ peaks, the BiOI peaks could be covered. It was observed that, with the rise of BiOI presence, the color of the composites changed gradually from white to yellow which could be taken as an evidence for the presence of BiOI.

XPS Analysis. The surface composition and metal oxidation state of the as-prepared composites were further analyzed by XPS. As can be seen from Figure 2a, only Bi, C, and O are detected over $\text{Bi}_2\text{O}_2\text{CO}_3$ but signals belonging to I are detected over BiOI and $\text{Bi}_2\text{O}_2\text{CO}_3/\text{BiOI}$. Even though CTAB is used as template, there is no sight of N1s signal at around 400 eV, confirming the complete removal of CTAB. The C1s peak (see Figure S1a in the Supporting Information) at a binding energy of ca. 284.6 eV is attributed to the signal from contaminant carbon.³⁹ The peak observed at 288.5 eV is ascribed to the carbon of carbonate in $\text{Bi}_2\text{O}_2\text{CO}_3$.^{40–42} The peaks located at 159.0 and 164.2 eV are assigned to $\text{Bi}4f_{7/2}$ and $\text{Bi}4f_{5/2}$, respectively (See Figure S1b, Supporting Information), which is the characteristic of Bi^{3+} in the achieved samples. It is clear that $\text{Bi}4f_{7/2}$ and $\text{Bi}4f_{5/2}$ binding energies of BiOI are lower than those of $\text{Bi}_2\text{O}_2\text{CO}_3$, indicating that the Bi^{3+} ions of BiOI and $\text{Bi}_2\text{O}_2\text{CO}_3$ are different in chemical environment. Figure 2b shows the high-resolution XPS spectrum of the I3d region, and the peaks at 618.5 and 630.1 eV are ascribed to the $\text{I}3d_{5/2}$ and $\text{I}3d_{3/2}$ photoemission, respectively. As one can see, the I3d peaks detected over the $\text{Bi}_2\text{O}_2\text{CO}_3/\text{BiOI}$ composites show binding energy similar to that of pure BiOI, and the results further confirm the presence of BiOI in the as-prepared composites.

Morphology and Microstructure. As can be seen from Figure 3, the samples are composed from dozens of nanoplates, showing morphologies that are flower-like. The thickness of the nanoplates in BiOI and $\text{Bi}_2\text{O}_2\text{CO}_3$ are about 60 nm. As for the $\text{Bi}_2\text{O}_2\text{CO}_3/\text{BiOI}$ composites, with a change of $\text{Bi}^{3+}/\text{CO}_3^{2-}/\text{I}^-$ ratio from 1/7/1 to 1/4/4 (i.e., an increase of I⁻ amount), there is a decline in nanoplate thickness and crinkling of nanoplate edges. The presence of I in the as-prepared samples is further confirmed by EDS (Figure 3f), and the weight

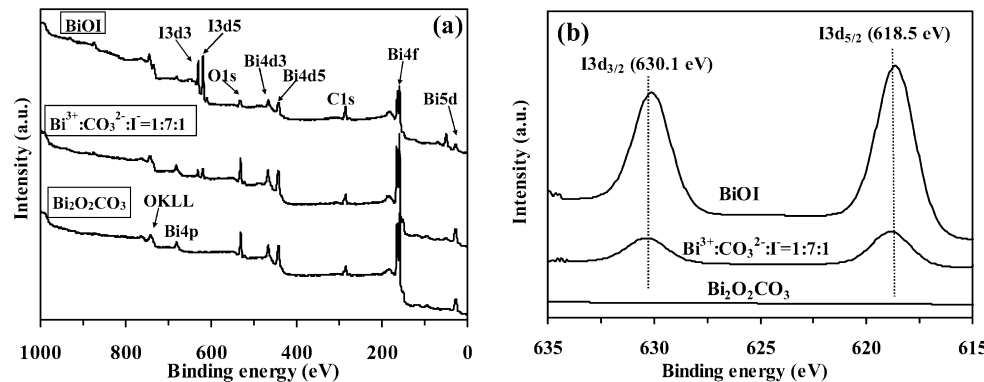


Figure 2. XPS spectra of as-prepared samples: (a) typical survey and (b) I3d core.

percentages of I are 1.3%, 3.2%, 11.1%, and 36.5% in composites prepared with $\text{Bi}^{3+}/\text{CO}_3^{2-}/\text{I}^- = 1/7/1$, 1/6/2, and 1/4/4 and pure BiOI. Although the content of I in the pure BiOI is a little higher than the theoretical value in BiOI (36.1%), it is within the limits of experimental error. The content of I in the composites increased by increasing the amount of KI employed in the preparation process, but I^- has not precipitated completely, indicating the competitive reaction between I^- and CO_3^{2-} to generate BiOI and $\text{Bi}_2\text{O}_2\text{CO}_3$.

The structure of the $\text{Bi}_2\text{O}_2\text{CO}_3/\text{BiOI}$ composite with molar ratio of $\text{Bi}^{3+}/\text{CO}_3^{2-}/\text{I}^- = 1/7/1$ was investigated by TEM and HRTEM. Consistent with the SEM results, the low-magnification TEM image in Figure 4a shows a flower-like morphology. As shown in Figure 4b, the HRTEM image clearly shows interfaces with *d*-spacings of tetragonal BiOI and $\text{Bi}_2\text{O}_2\text{CO}_3$. The fringes of $d = 0.190 \text{ nm}$ and $d = 0.459 \text{ nm}$ are in agreement with the (020) crystallographic plane of $\text{Bi}_2\text{O}_2\text{CO}_3$ (0.193 nm) and the (002) crystallographic plane of BiOI (0.458 nm), respectively. It is apparent that there are heterojunctions between BiOI and $\text{Bi}_2\text{O}_2\text{CO}_3$ in the as-synthesized composite.

Nitrogen Adsorption and Desorption Analysis. Listed in Table 1 are the special surface areas of relevant samples. The specific surface area of $\text{Bi}_2\text{O}_2\text{CO}_3$ and BiOI are 15.2 and 7.0 m^2/g , respectively, while those of $\text{Bi}_2\text{O}_2\text{CO}_3/\text{BiOI}$ composites with $\text{Bi}^{3+}/\text{CO}_3^{2-}/\text{I}^-$ molar ratio = 1/7/1, 1/6/2, and 1/4/4 are 21.0, 26.9, and 34.1 m^2/g (Table 1). Additionally, the $\text{Bi}_2\text{O}_2\text{CO}_3/\text{BiOI}$ samples show a type II adsorption–desorption isotherm with a distinct hysteresis loop in the $p/p_0 = 0.8–1$ range, which are typical characteristics of porous materials (see Figure S2, Supporting Information).

Optical Properties. Figure 5 shows the typical UV–visible absorption spectra of as-synthesized samples. Pure $\text{Bi}_2\text{O}_2\text{CO}_3$ sample can absorb UV light ($\lambda \leq 400 \text{ nm}$), while BiOI can absorb almost all visible light ($\lambda \leq 700 \text{ nm}$). It is clear that, with the increase of BiOI content in composites, there is an apparent red-shift and increase of absorption edges (determined by linear extrapolation of the steep part of UV–vis light absorption toward the baseline). In addition to strong absorption in the UV-light region, all $\text{Bi}_2\text{O}_2\text{CO}_3/\text{BiOI}$ composites have absorption in the visible light region (Table 1). The band gap energy (E_g) is commonly used to evaluate the optical absorption performance of semiconductors. For a crystalline semiconductor, the optical absorption near band edge follows the formula $(\alpha h\nu)^n = A(h\nu - E_g)$ where α , h , ν , E_g , and A are the absorption coefficient, Plank constant, light frequency, band gap, and a constant, respectively.^{33,36,38} Among them, n is 2 for

direct interband transition and 1/2 for indirect interband transition. For both, $\text{Bi}_2\text{O}_2\text{CO}_3$ and BiOI are direct interband transitions;^{33,36} the value of n equals 2. The E_g value can be estimated by extrapolating the straight portion of $(\alpha h\nu)^2 - (h\nu)$ plot to the $\alpha = 0$ point, and the relevant results are listed in Table 1. The band gaps of $\text{Bi}_2\text{O}_2\text{CO}_3$ and BiOI are 3.4 and 1.9 eV, respectively, quite consistent with the reported values.^{33,36,38} On the other hand, the E_g values of all the composites are smaller than that of $\text{Bi}_2\text{O}_2\text{CO}_3$, indicating that the composites are more efficient in absorbing visible light than $\text{Bi}_2\text{O}_2\text{CO}_3$ itself.

Photocatalytic Activity. Rh-B was adopted as a probe dye to evaluate the photocatalytic activity of the as-prepared samples under visible light. The variations of Rh-B concentration (C/C_0 , C is the concentration of Rh-B at irradiation time t , C_0 is the initial concentration of Rh-B: $2 \times 10^{-5} \text{ mol/L}$) versus irradiation time over the as-prepared samples are shown in Figure 6. The degradation rate was evaluated by the reaction constant k that can be determined by plotting $\ln(C_e/C)$ against irradiation time (C_e is the concentration of dye after the establishment of adsorption–desorption equilibrium). The k values of the samples are also listed in Table 1. One can see from Figure 6 that Rh-B can be completely removed by BiOI, $\text{Bi}_2\text{O}_2\text{CO}_3$, and $\text{Bi}_2\text{O}_2\text{CO}_3/\text{BiOI}$ composites in 60, 80, and 15 min, respectively, under the irradiation of visible light ($\lambda \geq 420 \text{ nm}$). The photocatalytic activities of the $\text{Bi}_2\text{O}_2\text{CO}_3/\text{BiOI}$ composites are, respectively, 6 and 7 times higher than that of individual BiOI and $\text{Bi}_2\text{O}_2\text{CO}_3$ (see the k values in Table 1); even considering the effect of specific surface area, it is still 2 and 5 times higher than that of individual BiOI and $\text{Bi}_2\text{O}_2\text{CO}_3$ (see the k/S_{BET} values in Table 1). The degradation rate of the $\text{Bi}_2\text{O}_2\text{CO}_3/\text{BiOI}$ composites is 8 times higher than that of BiOI under visible light,³³ and 3–7 times higher than that of $\text{Bi}_2\text{O}_2\text{CO}_3$ under solar light.^{37,38} It is considered that the formation of heterojunction structures between BiOI and $\text{Bi}_2\text{O}_2\text{CO}_3$ contributes most to its outstanding performances.

Furthermore, the amount of adsorbed Rh-B on the $\text{Bi}_2\text{O}_2\text{CO}_3/\text{BiOI}$ composites is much higher than that adsorbed on BiOI or $\text{Bi}_2\text{O}_2\text{CO}_3$. With the increase of BiOI in the composites, there is a decrease in band gap values and a rise in specific surface area as well as in the amount of adsorbed Rh-B. Considering that the degradation rates are similar among the three $\text{Bi}_2\text{O}_2\text{CO}_3/\text{BiOI}$ composites (Table 1), we speculate that the changes of special surface area and band gap are not the main reasons for the outstanding catalytic performance for dye removal. Interestingly, although the Rh-B in the aqueous solution can be totally removed by each of the as-prepared

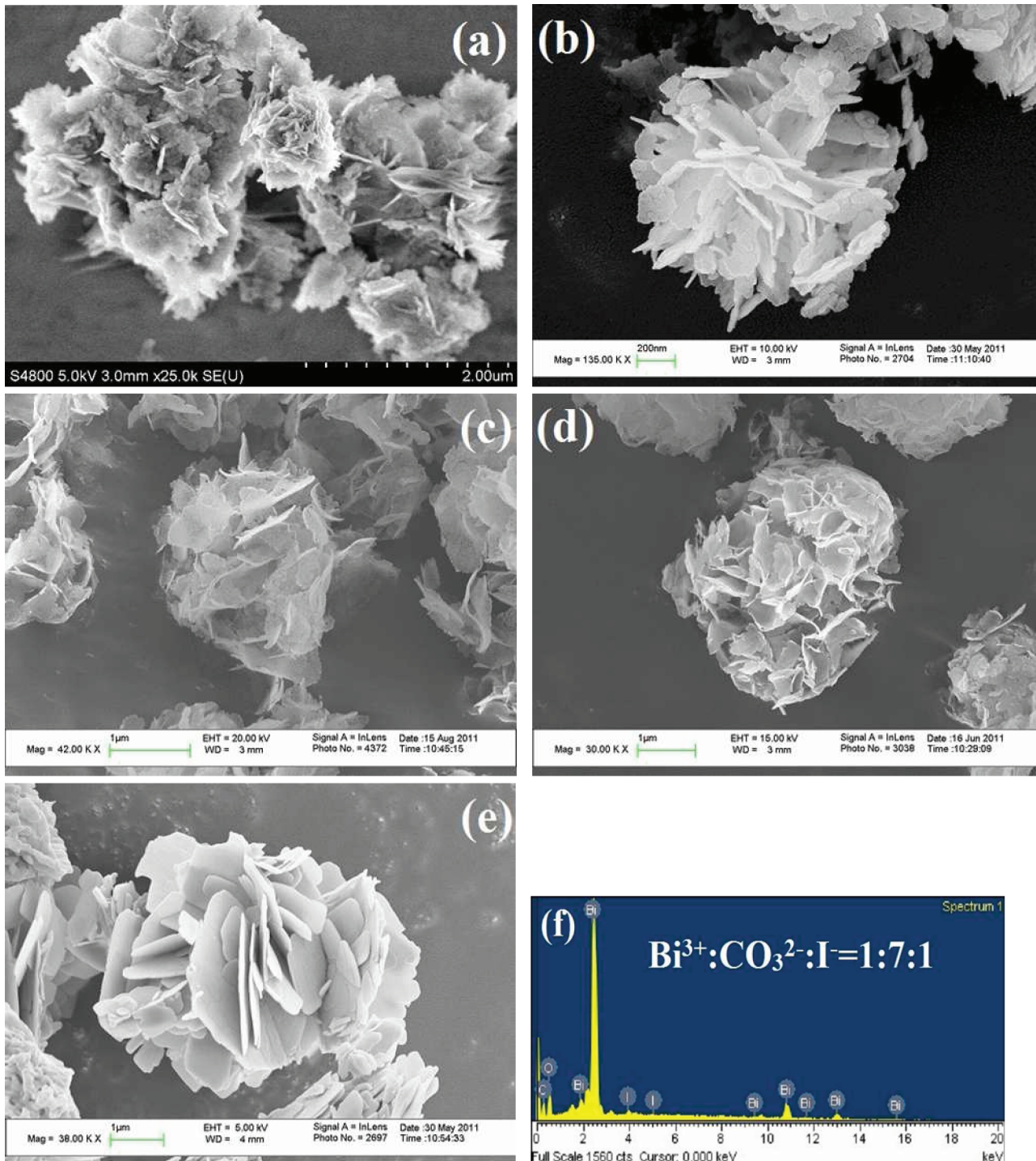


Figure 3. FESEM images of as-prepared samples: (a) $\text{Bi}_2\text{O}_2\text{CO}_3$, (b) $\text{Bi}_2\text{O}_2\text{CO}_3/\text{BiOI}$ ($\text{Bi}^{3+}/\text{CO}_3^{2-}/\text{I}^- = 1/7/1$), (c) $\text{Bi}_2\text{O}_2\text{CO}_3/\text{BiOI}$ ($\text{Bi}^{3+}/\text{CO}_3^{2-}/\text{I}^- = 1/6/2$), (d) $\text{Bi}_2\text{O}_2\text{CO}_3/\text{BiOI}$ ($\text{Bi}^{3+}/\text{CO}_3^{2-}/\text{I}^- = 1/4/4$), and (e) BiOI; (f) EDS spectrum of $\text{Bi}_2\text{O}_2\text{CO}_3/\text{BiOI}$ ($\text{Bi}^{3+}/\text{CO}_3^{2-}/\text{I}^- = 1/7/1$).

composites, the dye adsorbed on $\text{Bi}_2\text{O}_2\text{CO}_3/\text{BiOI}$ with molar ratio $\text{Bi}^{3+}/\text{CO}_3^{2-}/\text{I}^- = 1/6/2$ and $1/4/4$ cannot be decomposed. On the basis of the activity results, we deduced that the $\text{Bi}_2\text{O}_2\text{CO}_3/\text{BiOI}$ composite with a molar ratio of $\text{Bi}^{3+}/\text{CO}_3^{2-}/\text{I}^- = 1/7/1$ performed the best. By prolonging the irradiation time, the absorption peaks of Rh-B decrease and disappear, and there are no new peaks in the UV and visible region (see Figure S3a,b, Supporting Information). The results suggest that, in the presence of $\text{Bi}_2\text{O}_2\text{CO}_3/\text{BiOI}$ or $\text{Bi}_2\text{O}_2\text{CO}_3$, Rh-B can be completely removed. It seemed unreasonable that with such a

wide band gap the $\text{Bi}_2\text{O}_2\text{CO}_3$ samples could be excited under the irradiation of visible light. However, there were some similar reports that $\text{Bi}_2\text{O}_2\text{CO}_3$ samples could be excited under visible light or UV light.^{36–38,43} As reported by Zhao et al.,⁴³ about 87% of Rh-B could be removed in 15 min on plate-like $\text{Bi}_2\text{O}_2\text{CO}_3$ sample under visible light irradiation even with a wide band gap of 3.34 eV. It is deduced that the Rh-B dyes adsorbed on the surface of $\text{Bi}_2\text{O}_2\text{CO}_3$ can absorb visible light and be excited to generate electrons. This process is similar to that of dye-sensitized solar light cells.⁴⁴ The excited electrons transfer

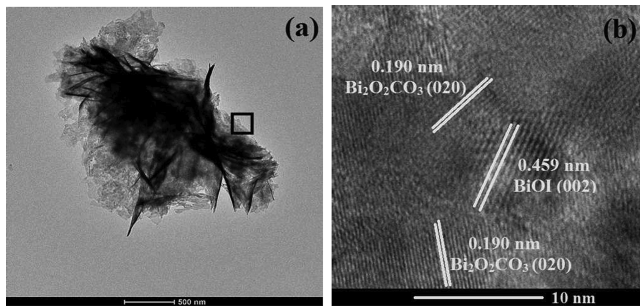


Figure 4. TEM and high-resolution TEM images of $\text{Bi}_2\text{O}_2\text{CO}_3/\text{BiOI}$ composite ($\text{Bi}^{3+}/\text{CO}_3^{2-}/\text{I}^- = 1/7/1$).

to the surface of $\text{Bi}_2\text{O}_2\text{CO}_3$, react with the absorbed O_2 and H_2O to generate $\cdot\text{OH}$, and finally mineralize dye molecule into CO_2 and H_2O . Therefore, even with wide band gap, the $\text{Bi}_2\text{O}_2\text{CO}_3$ sample still shows low photocatalytic activity under visible light irradiation. In the case of BiOI, the absorption peak at 553 nm diminishes gradually with irradiation time, while a new peak at around 510 nm increases slightly in intensity (see Figure S3c, Supporting Information). The results indicated that Rh-B cannot be completely decomposed on BiOI catalyst under the given conditions.

Wide Utilization and Recycling Property of Catalysts.

Factors such as recycling and wide utilization are essential factors for industrial application of photocatalysts. MB and crystal violet were adopted to study the universal usage of $\text{Bi}_2\text{O}_2\text{CO}_3/\text{BiOI}$ composite ($\text{Bi}^{3+}/\text{CO}_3^{2-}/\text{I}^- = 1/7/1$). First, one can see from Figure 7a that photolysis of MB is negligible. After exposure to visible light ($\lambda \geq 420 \text{ nm}$) for 80 min, 95%, 63%, and 37% of MB can be removed in the cases of $\text{Bi}_2\text{O}_2\text{CO}_3/\text{BiOI}$ composite, $\text{Bi}_2\text{O}_2\text{CO}_3$, and BiOI, respectively. Figure 7b shows the plotting of $\ln(C_e/C)$ versus irradiation time. The linear relationship between $\ln(C_e/C)$ and irradiation time suggests that the photodegradation of MB over these catalysts is first-order. The reaction rate constant is 0.36 min^{-1} on $\text{Bi}_2\text{O}_2\text{CO}_3/\text{BiOI}$ composite, 3 and 7 times that on $\text{Bi}_2\text{O}_2\text{CO}_3$ and BiOI, respectively. Figure 7c demonstrates the photocatalytic performances of the catalysts in removing crystal violet under visible light. It is clear that the $\text{Bi}_2\text{O}_2\text{CO}_3/\text{BiOI}$ composite performs much better than its individual components, similar to the cases of Rh-B and MB degradation. The time involved in complete removal of these three kinds of dye differed from each other, and this may be attributed to the difference in the molecular structures which resulted in a different degradation mechanism.³³

The performance of the $\text{Bi}_2\text{O}_2\text{CO}_3/\text{BiOI}$ composite for the treatment of wastewater containing more than one kind of dye was also investigated. The total concentration of Rh-B, MB, and crystal violet was $2 \times 10^{-5} \text{ mol/L}$ (catalyst: 50 mg). The absorption peaks of Rh-B, MB, and crystal violet could be

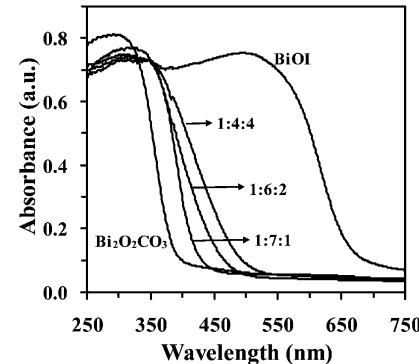


Figure 5. UV-vis diffuse reflectance spectra of $\text{Bi}_2\text{O}_2\text{CO}_3$, BiOI, and $\text{Bi}_2\text{O}_2\text{CO}_3/\text{BiOI}$ composites.

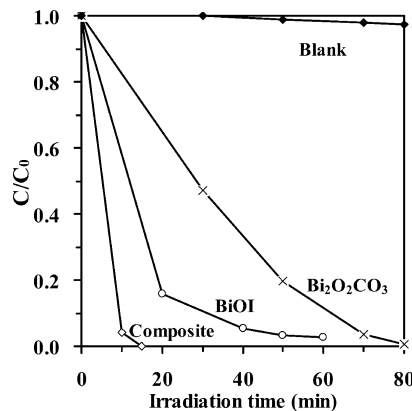


Figure 6. Photocatalytic activities of the as-prepared samples toward the degradation of Rh-B under visible-light irradiation.

indexed by making comparison with the UV-vis absorption spectra (see Figure S4a, Supporting Information). It is clear that all of the dyes can be completely removed after 60 min under visible light (Figure 7d). However, using BiOI and $\text{Bi}_2\text{O}_2\text{CO}_3$ under the same irradiation conditions, the extent of dye removal is only about 40% (see Figure S4b,c, Supporting Information), further confirming the priority of the composite photocatalyst to its component toward wastewater treatment.

The durability of the $\text{Bi}_2\text{O}_2\text{CO}_3/\text{BiOI}$ composite ($\text{Bi}^{3+}/\text{CO}_3^{2-}/\text{I}^- = 1/7/1$) was evaluated through the recycle of the used catalyst. For each cycle, catalyst was collected by centrifugation. There is no apparent loss of photocatalytic activity in removing crystal violet in the fifth cycle, and even in the 10th run, the decline in photocatalytic activity is less than 5% (see Figure 8). The used $\text{Bi}_2\text{O}_2\text{CO}_3/\text{BiOI}$ was also examined by XRD, and there is no detectable difference between the as-prepared and used samples (Figure 1b,c). Therefore, it can be deduced that the $\text{Bi}_2\text{O}_2\text{CO}_3/\text{BiOI}$ composite has good photostability.

Table 1. Results of BET Surface Area, Absorption Edges, Band Gaps, Amount of Rh-B Adsorbed, and Rh-B Photodegradation Rates over the As-Prepared Samples

samples	S_{BET} ($\text{m}^2 \cdot \text{g}^{-1}$)	absorption edge (nm)	band gap (eV)	adsorbed Rh-B (%)	k (min^{-1})	k/S_{BET} ($\text{g} \cdot \text{min}^{-1} \cdot \text{m}^{-2}$)
$\text{Bi}_2\text{O}_2\text{CO}_3$	15.2	388	3.4	10.2	0.0504	0.0033
$\text{Bi}^{3+}/\text{CO}_3^{2-}/\text{I}^- = 1/7/1$	21.0	428	3.2	43.1	0.3623	0.0173
$\text{Bi}^{3+}/\text{CO}_3^{2-}/\text{I}^- = 1/6/2$	26.9	470	3.0	85.6	0.3406	0.0151
$\text{Bi}^{3+}/\text{CO}_3^{2-}/\text{I}^- = 1/4/4$	34.1	500	2.8	97.4	0.3402	0.0100
BiOI	7.0	670	1.9	28.7	0.0600	0.0086

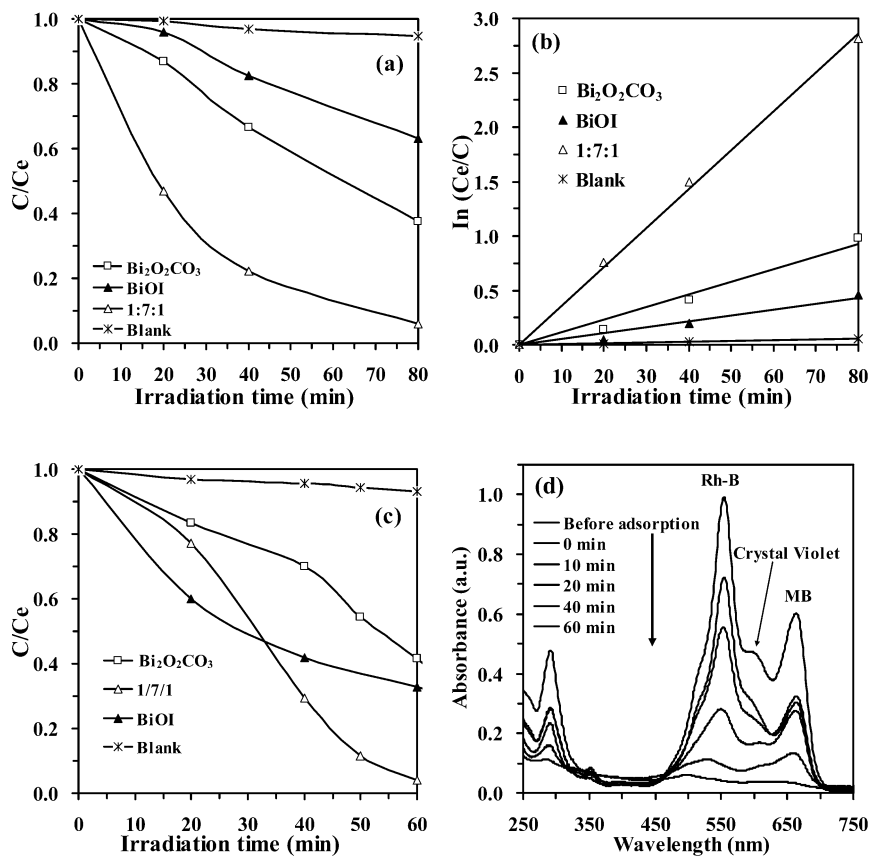


Figure 7. (a) Photocatalytic degradation of MB and (b) relevant degradation rates in the presence of as-prepared samples. ($\text{Bi}_2\text{O}_2\text{CO}_3/\text{BiOI}$ composite, $k = 0.036 \text{ min}^{-1}$, $R^2 = 0.9979$; BiOI , $k = 0.005 \text{ min}^{-1}$, $R^2 = 0.9758$; $\text{Bi}_2\text{O}_2\text{CO}_3$, $k = 0.012 \text{ min}^{-1}$, $R^2 = 0.9842$), (c) photocatalytic degradation of crystal violet, (d) photodegradation of mixed dye containing wastewater on $\text{Bi}_2\text{O}_2\text{CO}_3/\text{BiOI}$ composite ($\text{Bi}^{3+}/\text{CO}_3^{2-}/\text{I}^- = 1/7/1$).

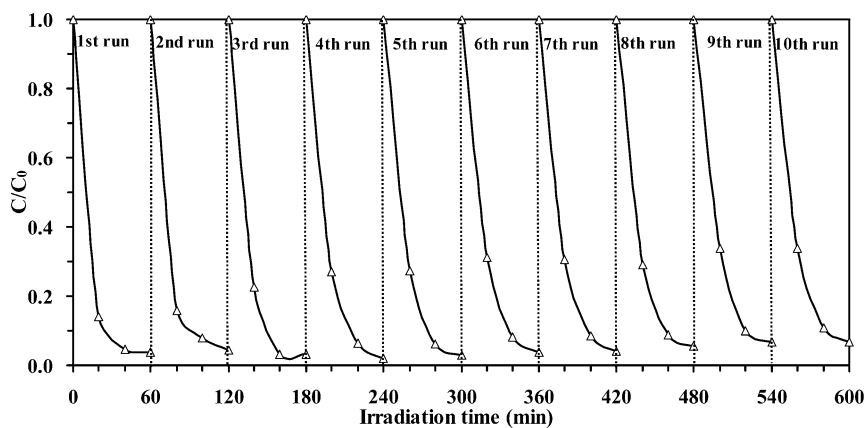


Figure 8. Recycling property of the composite photocatalyst ($\text{Bi}^{3+}/\text{CO}_3^{2-}/\text{I}^- = 1/7/1$).

Relationship between Photocatalytic Activity and Structure. $\text{Bi}_2\text{O}_2\text{CO}_3/\text{BiOI}$ shows excellent catalytic efficiency toward the photodegradation of the dyes under visible light irradiation. It is very important to disclose the relationship of its catalytic performance and structure or surface property. It is clear that, despite an increase of specific surface areas of the composites with the increase of BiOI content, there is no improvement of photocatalytic activity of $\text{Bi}_2\text{O}_2\text{CO}_3/\text{BiOI}$ with rise of specific surface area. Thus, we can deduce that the surface area shows little effect on the photocatalytic performance of the composite catalyst. In addition, there is no direct correlation between the catalytic efficiency and the crystallinity

(XRD result) or morphology (SEM result) or optical property (UV-visible absorption result). However, the high-resolution TEM image demonstrates there are many heterojunctions of $\text{Bi}_2\text{O}_2\text{CO}_3/\text{BiOI}$ in the composite. Li and co-workers reported that the surface phase junctions formed between the anatase and rutile phase of TiO_2 (or heterogeneous junctions between MoS_2 and CdS) can greatly enhance the photocatalytic activity for H_2 production, which is beneficial for the separation of photoexcited electrons and holes.^{45,46} Zhang and coauthors deduced that the formation of heterojunction between BiOI and TiO_2 was the main reason in improving photocatalytic activity in dye removal.¹³ Other researchers also regarded that

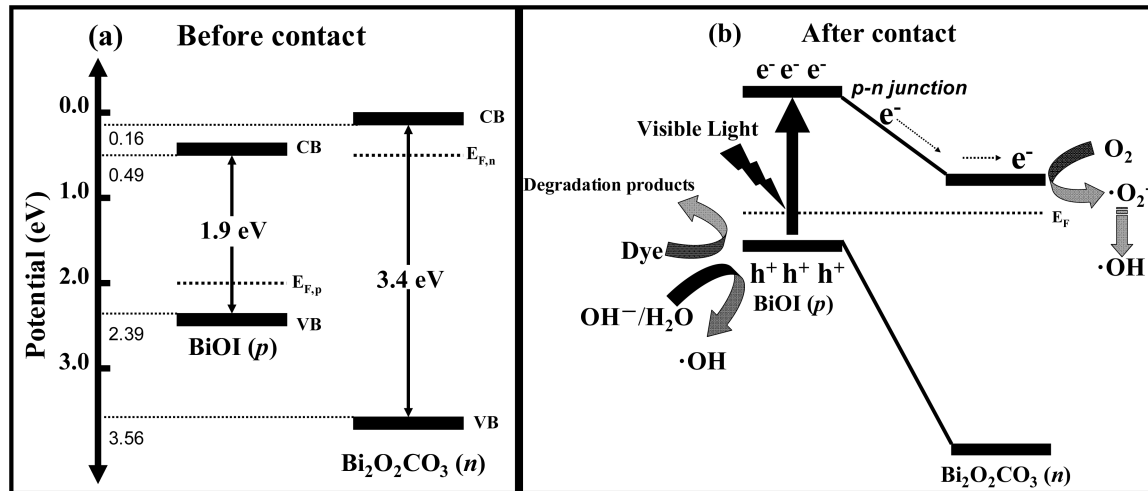


Figure 9. Schematic diagrams for (a) energy band of $\text{Bi}_2\text{O}_2\text{CO}_3$ and BiOI and (b) the formation of $p-n$ junction and the possible charge separation process.

the formation of heterojunction structures could enhance photocatalytic activities in dye degradation.^{12,15,18,20} Therefore, it is considered that the superiority of the composite photocatalyst can be attributed to the heterojunction structures between BiOI and $\text{Bi}_2\text{O}_2\text{CO}_3$.

It is generally accepted that the photogenerated electrons and holes transfer to the surface to react with the adsorbed reactants, and the migration direction of the photogenerated charge carriers depends on the band edge position of semiconductors. The conduction band (CB) and valence band (VB) potential of BiOI and $\text{Bi}_2\text{O}_2\text{CO}_3$ at the point of zero charge were calculated by Butler and Ginley using eqs 1 and 2:¹³

$$E_{\text{VB}} = X - E^{\text{e}} + 0.5E_{\text{g}} \quad (1)$$

$$E_{\text{CB}} = E_{\text{VB}} - E_{\text{g}} \quad (2)$$

where X is the absolute electronegativity of the semiconductors, which is defined as the geometric average of the absolute electronegativity of the constituent atoms; E^{e} is the energy of free electrons on the hydrogen scale (ca. 4.5 eV); E_{VB} is the VB edge potential; and the E_{g} is the band gap of the semiconductor. The X values of BiOI and $\text{Bi}_2\text{O}_2\text{CO}_3$ are ca. 5.94 and 6.36 eV, and the top of the VB and the bottom of the CB of BiOI are calculated to be 2.39 and 0.49 eV, respectively, according to the above equations. On the basis of the above data, the VB and CB of the $\text{Bi}_2\text{O}_2\text{CO}_3$ are estimated to be 3.56 and 0.16 eV, respectively.

The energy band structures of BiOI and $\text{Bi}_2\text{O}_2\text{CO}_3$ are schematically illustrated in Figure 9a. The p -type BiOI is with Fermi energy level close to the valence band¹³ while the n -type $\text{Bi}_2\text{O}_2\text{CO}_3$ is with Fermi energy level close to the conduction band. When the two semiconductors are in contact, the CB potential of $\text{Bi}_2\text{O}_2\text{CO}_3$ is more negative than that of BiOI. There is hence diffusion of electrons from $\text{Bi}_2\text{O}_2\text{CO}_3$ to BiOI, resulting in accumulation of negative charges in BiOI close to the junction. At the same time, the holes transfer from BiOI to $\text{Bi}_2\text{O}_2\text{CO}_3$, leaving a positive section in $\text{Bi}_2\text{O}_2\text{CO}_3$ near the junction. With equilibration of BiOI and $\text{Bi}_2\text{O}_2\text{CO}_3$ Fermi levels, the diffusion of electrons from $\text{Bi}_2\text{O}_2\text{CO}_3$ to BiOI stops. Meanwhile, the energy bands of BiOI shift upward along the Fermi level (E_{Fp}) and those of the $\text{Bi}_2\text{O}_2\text{CO}_3$ shift downward

along its Fermi level (E_{Fn}) (Figure 9b). Under the irradiation of visible-light, BiOI is excited and there is the generation of electron–hole pairs. According to the schema of Figure 9b, the excited electrons on the CB of BiOI transfer to the CB of $\text{Bi}_2\text{O}_2\text{CO}_3$, while the excited holes remain on the VB of BiOI. Furthermore, the migration of photogenerated electrons and holes could be promoted by the internal electric field. Therefore, the formation of $p-n$ ($\text{Bi}_2\text{O}_2\text{CO}_3/\text{BiOI}$) heterojunctions on the surface could effectively separate the photoexcited electron–hole pairs and could greatly reduce the recombination of the photogenerated charge carries. Consequently, there is free transfer of the separated electrons and holes toward the surface. It follows that the electrons react with the adsorbed O_2 to generate $\cdot\text{O}_2^-$ and subsequently H_2O_2 . There is the formation of $\cdot\text{OH}$ radicals (Eqs 3–5) when H_2O_2 picks up an electron and a hole reacts with OH^- (Eq 6).⁴⁷ It has been reported that h^+ , $\cdot\text{OH}$, and $\cdot\text{O}_2^-$ have high oxidation ability and react with dyes to intermediates and finally to CO_2 and H_2O .^{48–50}

It was reported that the active species could be different across different catalysts. For example, Wang et al. attributed the degradation of BPA over Bi_2WO_6 to photogenerated holes rather than $\cdot\text{OH}$ radicals.⁵⁰ However, Zhang and co-workers suggested that both direct hole and $\cdot\text{OH}$ oxidation have an important role to play in the photodecomposition of MO over BiOI.⁴⁷ It was suggested that $\cdot\text{OH}$ is generated from O_2 and photogenerated electrons according to the following steps:



To clarify the degradation mechanism, triethanolamine (TEOA) and *tert*-butyl alcohol (TBA) were adopted as hole and $\cdot\text{OH}$ scavenger in the present work, respectively. Before irradiation, these scavengers (kept at 10 mmol/L) were added to the MB solutions together with the catalysts. As can be seen in Figure S5 (Supporting Information), the degradation efficiency of MB decreases from 95% to 55% and from 95% to 0% with the addition of TEOA and TBA, respectively,

indicating that the decomposition of MB is mainly due to ·OH. The decrease of photocatalytic efficiency from 94% to 55% could be owing to the fact that ·OH was generated by two ways as displayed in Figure 9, and the addition of the hole scavenger can inhibit the generation of ·OH from holes (eq 6) whereas the ·OH generated from electrons (eq 5) remained intact.

CONCLUSIONS

With the assistance of CTAB, the $\text{Bi}_2\text{O}_2\text{CO}_3/\text{BiOI}$ composite photocatalyst with flower-like morphology was successfully synthesized at room temperature by a facile method. It shows excellent photocatalytic activities in the degradation of Rh-B, MB, crystal violet, or a mixture of the three dyes under the irradiation of visible light ($\lambda \geq 420 \text{ nm}$). The photostability and recyclability of the composite are good. The excellent catalytic efficiency is suggested to be closely related to the $\text{Bi}_2\text{O}_2\text{CO}_3/\text{BiOI}$ heterojunctions which are generally regarded to be favorable for the separation of photogenerated electrons and holes. The active species in MB degradation was found to be ·OH rather than holes. In other words, the ·OH radicals produced from both photogenerated holes and electrons take part in dye decomposition, and the composite catalyst has the potential for industrial application.

ASSOCIATED CONTENT

Supporting Information

Figures S1–S5. This material is available free of charge via the Internet at <http://pubs.acs.org>.

AUTHOR INFORMATION

Corresponding Author

*Phone: 86-731-88821310. Fax: 86-731-88821310. E-mail: sf_yin@hnu.edu.cn.

Notes

The authors declare no competing financial interest.

ACKNOWLEDGMENTS

This project was financially supported by Hunan Provincial Natural Science Foundation of China (10JJ1003), NSFC (20873038, J0830415), the program for New Century Excellent Talents in Universities (NCET-10-0371), and the Fundamental Research Funds for the Central Universities.

REFERENCES

- Chen, X. B.; Mao, S. S. Titanium dioxide nanomaterials: synthesis, properties, modifications, and applications. *Chem. Rev.* **2007**, *107*, 2891.
- Walter, M. G.; Warren, E. L.; McKone, J. R.; Boettcher, S. W.; Mi, Q. X.; Santori, E. A.; Lewis, N. S. Solar water splitting cells. *Chem. Rev.* **2010**, *110*, 6446.
- Zou, Z. G.; Ye, J. H.; Sayama, K.; Arakawa, H. Direct splitting of water under visible light irradiation with an oxide semiconductor photocatalyst. *Nature* **2001**, *414*, 625.
- Asahi, R.; Morikawa, T.; Ohwaki, T.; Aoki, K.; Taga, Y. Visible-light photocatalysis in nitrogen-doped titanium oxides. *Science* **2001**, *293*, 269.
- Osterloh, F. E. Inorganic materials as catalysts for photochemical splitting of water. *Chem. Mater.* **2008**, *20*, 35.
- Song, S. Y.; Zhang, Y.; Xing, Y.; Wang, C.; Feng, J.; Shi, W. D.; Zheng, G. L.; Zhang, H. J. Rectangular AgIn(WO₄)₂ nanotubes: a promising photoelectric material. *Adv. Funct. Mater.* **2008**, *18*, 2328.
- Chen, X. B.; Shen, S. H.; Guo, L. J.; Mao, S. S. Semiconductor-based photocatalytic hydrogen generation. *Chem. Rev.* **2010**, *110*, 6503.
- Yasukaka, K.; Hiromi, Y. Efficient photocatalytic degradation of organics diluted in water and air using TiO₂ designed with zeolites and mesoporous silica materials. *J. Mater. Chem.* **2011**, *21*, 2407.
- Kudo, A.; Miseki, Y. Heterogeneous photocatalyst materials for water splitting. *Chem. Soc. Rev.* **2009**, *38*, 253.
- Ladhe, R. D.; Baviskar, P. K.; Tan, W. W.; Zhang, J. B.; Cokhande, C. D.; Sankpal, B. R. LPG sensor based on complete inorganic n-Bi₂S₃-p-CuSCN heterojunction synthesized by a simple chemical route. *J. Phys. D: Appl. Phys.* **2010**, *43*, 245320.
- Liu, X. W.; Cao, H. Q.; Yin, J. F. Generation and photocatalytic activities of Bi@Bi₂O₃ microspheres. *Nano Res.* **2011**, *4*, 470.
- Zhou, Y.; Frumeich, F.; Heel, A.; Patzke, G. One-step hydrothermal coating approach to photocatalytically active oxide composites. *Dalton Trans.* **2010**, *39*, 6043.
- Zhang, X.; Zhang, L. Z.; Xie, T. F.; Wang, D. J. Low-temperature synthesis and high visible-light-induced photocatalytic activity of BiOI/TiO₂ heterostructures. *J. Phys. Chem. C* **2009**, *113*, 7371.
- Dai, G. P.; Yu, J. G.; Liu, G. Synthesis and enhanced visible-light photoelectrocatalytic activity of p-n junction BiOI/TiO₂ nanotube arrays. *J. Phys. Chem. C* **2011**, *115*, 7339.
- Cheng, H. F.; Huang, B. B.; Dai, Y.; Qin, X. Y.; Zhang, X. Y. One-step synthesis of the nanostructured AgI/BiOI composites with highly enhanced visible-light photocatalytic performances. *Langmuir* **2010**, *26*, 6618.
- Chai, S. Y.; Kin, Y. J.; Jung, M. H.; Chakraborty, A. K.; Jung, D.; Lee, W. I. Heterojunctioned BiOCl/Bi₂O₃, a new visible light photocatalyst. *J. Catal.* **2009**, *262*, 144.
- Chang, X. F.; Gang, Y.; Huang, J.; Li, Z.; Zhu, S. F.; Yu, P. F.; Cheng, C.; Deng, S. B.; Ji, G. B. Enhancement of photocatalytic activity over NaBiO₃/BiOCl composite prepared by an in situ formation strategy. *Catal. Today* **2010**, *153*, 193.
- Li, T. B.; Chen, G.; Zhou, C.; Shen, Z. Y.; Jin, R. C.; Sun, J. X. New photocatalyst BiOCl/BiOI composites with highly enhanced visible light photocatalytic performances. *Dalton Trans.* **2011**, *40*, 6751.
- Liu, Z. Y.; Sun, D. D.; Guo, P.; Leckie, J. O. An efficient bicomponent TiO₂/SnO₂ nanofiber photocatalyst fabricated by electrospinning with a side-by-side dual spinneret method. *Nano Lett.* **2007**, *7*, 1081.
- Wang, Z. Y.; Huang, B. B.; Dai, Y.; Qin, X. Y.; Zhang, X. Y.; Wang, P.; Liu, H. X.; Yu, J. X. Highly photocatalytic ZnO/In₂O₃ heteronanostructures synthesized by a coprecipitation method. *J. Phys. Chem. C* **2009**, *113*, 4612.
- Guan, M. L.; Ma, D. K.; Hu, S. W.; Chen, Y. J.; Huang, S. M. From hollow olive-shaped BiVO₄ to n-p core-shell BiVO₄@Bi₂O₃ microspheres: controlled synthesis and enhanced visible-light-responsive photocatalytic properties. *Inorg. Chem.* **2011**, *50*, 800.
- Yao, W. F.; Xu, X. H.; Wang, H.; Zhou, J. T.; Yang, X. N.; Zhang, Y.; Shang, S. X.; Huang, B. B. Photocatalytic property of perovskite bismuth titanate. *Appl. Catal., B* **2004**, *52*, 109.
- Zhou, L.; Wang, W. Z.; Xu, H. L.; Sun, S. M.; Shang, M. Bi₂O₃ hierarchical nanostructures: controllable synthesis, growth mechanism, and their application in photocatalysis. *Chem.—Eur. J.* **2009**, *15*, 1776.
- In, J.; Yoon, I.; Seo, K. Y.; Park, J. H.; Choo, J. B.; Lee, Y. H.; Kim, B. S. Polymorph-tuned synthesis of α- and β-Bi₂O₃ nanowires and determination of their growth direction from polarized raman single nanowire microscopy. *Chem.—Eur. J.* **2011**, *17*, 1304.
- Shamaila, S.; Leghari Sajjad, A. K.; Chen, F.; Zhang, J. L. Study on highly visible light active Bi₂O₃ loaded ordered mesoporous titania. *Appl. Catal., B* **2010**, *94*, 272.
- Zhang, C.; Zhu, Y. F. Synthesis of square Bi₂WO₆ nanoplates as high-activity visible-light-driven photocatalysts. *Chem. Mater.* **2005**, *17*, 3537.
- He, D. Q.; Wang, L. L.; Li, H. Y.; Yan, T. Y.; Wang, D. J.; Xie, T. F. Self-assembled 3D hierarchical clew-like Bi₂WO₆ microspheres: synthesis, photo-induced charges transfer properties, and photocatalytic activities. *CrystEngComm* **2011**, *13*, 4053.

- (28) Wang, C. Y.; Zhang, H.; Li, F.; Zhu, L. Y. Degradation and mineralization of bisphenol A by mesoporous Bi₂WO₆ under simulated solar light irradiation. *Environ. Sci. Technol.* **2010**, *44*, 6843.
- (29) Ke, D. N.; Peng, T. Y.; Ma, L.; Cai, P.; Dai, K. Effects of hydrothermal temperature on the microstructures of BiVO₄ and its photocatalytic O₂ evolution activity under visible light. *Inorg. Chem.* **2009**, *48*, 4685.
- (30) Wang, Z. Q.; Luo, W. J.; Yan, S. C.; Feng, J. Y.; Zhao, Z. Y.; Zhu, Y. S.; Li, Z. S.; Zou, Z. G. BiVO₄ nano-leaves: mild synthesis and improved photocatalytic activity for O₂ production under visible light irradiation. *CrystEngComm* **2011**, *13*, 2500.
- (31) Zhang, X.; Ai, Z. H.; Jia, F. L.; Zhang, L. Z. Generalized one-pot synthesis, characterization, and photocatalytic activity of hierarchical BiOX (X=Cl, Br, I) nanoplate microspheres. *J. Phys. Chem. C* **2008**, *112*, 747.
- (32) Deng, Z. T.; Chen, D.; Peng, B.; Tang, F. Q. From bulk Metal Bi to two-dimensional well-crystallized BiOX (X=Cl, Br) micro- and nanostructures: synthesis and characterization. *Cryst. Growth Des.* **2008**, *8*, 2995.
- (33) Lei, Y. Q.; Wang, G. H.; Song, S. Y.; Fan, W. Q.; Pang, M.; Tang, J. K.; Zhang, H. J. Room temperature, template-free synthesis of BiOI hierarchical structures: visible-light photocatalytic and electrochemical hydrogen storage properties. *Dalton Trans.* **2010**, *39*, 3273.
- (34) Xia, J. X.; Yin, S.; Li, H. M.; Xu, H.; Yan, Y. S.; Zhang, Q. Self-assembly and enhanced photocatalytic properties of BiOI hollow microspheres via a reactable ionic liquid. *Langmuir* **2011**, *27*, 1200.
- (35) Chen, R.; So, M. H.; Yang, J.; Deng, F.; Che, C. M.; Sun, H. Z. Fabrication of bismuth subcarbonate nanotube arrays from bismuth citrate. *Chem. Commun.* **2006**, *21*, 2265.
- (36) Cheng, H. F.; Huang, B. B.; Yang, K. S.; Wang, Z. Y.; Qin, X. Y.; Zhang, X. Y.; Dai, Y. Facile template-free synthesis of Bi₂O₂CO₃ hierarchical microflowers and their associated photocatalytic activity. *ChemPhysChem* **2010**, *11*, 2167.
- (37) Zheng, Y.; Duan, F.; Chen, M. Q.; Xie, Y. Synthetic Bi₂O₂CO₃ nanostructures: novel photocatalyst with controlled special surface exposed. *J. Mol. Catal. A: Chem.* **2010**, *317*, 34.
- (38) Liu, Y. Y.; Wang, Z. Y.; Huang, B. B.; Yang, K. S.; Zhang, X. Y.; Qin, X. Y.; Dai, Y. Preparation, electronic structure, and photocatalytic properties of Bi₂O₂CO₃ nanosheet. *Appl. Surf. Sci.* **2010**, *257*, 172.
- (39) Wang, H.; Z. Wu, Z.; Liu, Y. A simple two-step template approach for preparing carbon-doped mesoporous TiO₂ hollow microspheres. *J. Phys. Chem. C* **2009**, *113*, 13317.
- (40) Purkayastha, A.; Yan, Q. Y.; Raghuveer, M. S.; Gandhi, D. D.; Li, H. F.; Liu, Z. W.; Ramanujan, R. V.; Borca-Tasciuc, T.; Ramanath, G. Surfactant-directed synthesis of branched Bismuth Telluride/Sulfide core/shell nanorods. *Adv. Mater.* **2008**, *20*, 2679.
- (41) Chen, D. M.; Jiang, Z. Y.; Geng, J. Q.; Wang, Q.; Yang, D. D.; Carbon and nitrogen co-doped TiO₂ with enhanced visible-light photocatalytic activity. *Ind. Eng. Chem. Res.* **2007**, *46*, 2741.
- (42) Sun, H. Q.; Bai, Y.; Cheng, Y. P.; Jin, W. Q.; Xu, N. P. Preparation and characterization of visible-light-driven carbon–sulfur-codoped TiO₂ photocatalysts. *Ind. Eng. Chem. Res.* **2006**, *45*, 4971.
- (43) Zhao, T. Y.; Zai, J. T.; Xu, M.; Zou, Q.; Su, Y. Z.; Wang, K. X.; Qian, X. F. Hierarchical Bi₂O₂CO₃ microspheres with improved visible-light-driven photocatalytic activity. *CrystEngComm* **2011**, *13*, 4010.
- (44) Nazeeruddin, M. K.; Baranoff, E.; Grätzel, M. Dye-sensitized solar cells: A brief overview. *Sol. Energy* **2011**, *85*, 1172.
- (45) Zhang, J.; Xu, Q.; Feng, Z. C.; Li, C. Importance of the relationship between surface phases and photocatalytic activity of TiO₂. *Angew. Chem., Int. Ed.* **2008**, *47*, 1766.
- (46) Zong, X.; Yan, H. J.; Wu, G. P.; Ma, G. J.; Wen, F. Y.; Wang, L.; Li, C. Enhancement of photocatalytic H₂ evolution on CdS by loading MoS₂ as cocatalyst under visible light irradiation. *J. Am. Chem. Soc.* **2008**, *130*, 7176.
- (47) Wang, Y. N.; Deng, K. J.; Zhang, L. Z. Visible light photocatalysis of BiOI and its photocatalytic activity enhancement by *in situ* ionic liquid modification. *J. Phys. Chem. C* **2011**, *115*, 14300.
- (48) Hu, Y.; Li, D. Z.; Zheng, Y.; Chen, W.; He, Y. H.; Shao, Y.; Fu, X. Z.; Xiao, G. C. BiVO₄/TiO₂ nanocrystalline heterostructure: A wide spectrum responsive photocatalyst towards the highly efficient decomposition of gaseous benzene. *Appl. Catal., B* **2011**, *104*, 30.
- (49) Guo, C. S.; Ge, M.; Liu, L.; Gao, G. D.; Feng, Y. C.; Wang, Y. Q. Directed synthesis of mesoporous TiO₂ microspheres: catalysts and their photocatalysis for bisphenol A degradation. *Environ. Sci. Technol.* **2010**, *44*, 419.
- (50) Wang, C. Y.; Zhang, H.; Li, F.; Zhu, L. Y. Degradation and mineralization of bisphenol A by mesoporous Bi₂WO₆ under simulated solar light irradiation. *Environ. Sci. Technol.* **2010**, *44*, 6843.